Dalton Transactions

Water-soluble Dinuclear Iridium(III) and Ruthenium(II) Bis-terdentate Complexes: Photophysics and Electrochemiluminescence

Journal:	*Dalton Transactions*
Manuscript ID	DT-ART-07-2022-002104.R1
Article Type:	Paper
Date Submitted by the Author:	09-Aug-2022
Complete List of Authors:	Liu, Bingqing; Indiana University Bloomington, Chemistry Yang, Xin; Tianjin University of Technology Jabed, Mohammed; Colorado State University, Chemistry Kilina, Svetlana; North Dakota State University, Chemistry and Biochemistry Yang, Zhengchun; Tianjin University of Technology Sun, Wenfang; North Dakota State University, Chemistry

Dalton Transactions

ARTICLE

Water-soluble Dinuclear Iridium(III) and Ruthenium(II) Bis-terdentate Complexes: Photophysics and Electrochemiluminescence

Received 00th January 20xx,
Accepted 00th January 20xx

DOI: 10.1039/x0xx00000x

Bingqing Liu,[a] Xin Yang,[b] Mohammed Jabed,[a] Svetlana Kilina,[a] Zhengchun Yang,*[,b] Wenfang Sun*[,a]

The synthesis, photophysics, and electrochemiluminescence (ECL) of four water-soluble dinuclear Ir(III) and Ru(II) complexes (**1**–**4**) terminally-capped by 4′-phenyl-2,2′:6′,2″-terpyridine (tpy) or 1,3-di(pyrid-2-yl)-4,6-dimethylbenzene (N^C^N) ligands and linked by a 2,7-bis(2,2′:6′,2″-terpyridyl)fluorene with oligoether chains on C9 are reported. The impact of the tpy or N^C^N ligands and metal centers on the photophysical properties of **1**–**4** was assessed by spectroscopic methods including UV–vis absorption, emission, and transient absorption, and by time-dependent density functional theory (TDDFT) calculations. These complexes exhibited distinct singlet and triplet excited-state properties upon variation of the terminal-capping terdentate ligands and the metal centers. The ECL properties of the three water-soluble complexes **1**–**3** were investigated in neutral phosphate buffer solutions (PBS) by adding tripropylamine (TPA) as a co-reactant, and the observed ECL intensity followed the descending order of **3** > **1** > **2**. Complex **3** bearing the $[Ru(tpy)_2]^{2+}$ units displayed more pronounced ECL signals, rendering its analogues great potential for further ECL study.

Introduction

Electrochemiluminescence (ECL), a well-known approach for generation of emission, has attracted extensive interest over the past decade, in which a high-energy electron-transfer reaction of electrogenerated species at the surfaces of electrodes occurs to form emitting excited states.[1-4] ECL has been widely employed in various applications, such as light-emitting devices,[5] sensors for food analysis,[6] and bioanalysis,[7] etc. To date, the ECL emitters investigated include organic dyes, inorganic metal complexes, and semiconductor nanomaterials.[1-4] Pioneered by Bard and co-workers' work, tris(bipyridyl)ruthenium(II) complex ($[Ru(bpy)_3]^{2+}$) and its derivatives have drawn great attention as promising ECL candidates because of their high photoluminescence efficiencies and good photostability.[8,9] With high sensitivity and fast response, $Ru(bpy)_3^{2+}$-based ECL probe has been successfully developed for bioanalytical applications.[10] The practical potential of these Ru(II) complexes as ECL probes, however, is limited by their narrow range of emission at 600 − 650 nm. A variety of Ir(III) complexes, therefore, have been developed as emerging ECL materials owing to their enhanced phosphorescence quantum yields, long-lived triplet excited states, and readily tunable emitting colors spanning from the deep blue to NIR regions.[11-13] Unfortunately, most of the reported ECL Ir(III) and Ru(II) complexes can only dissolve in organic solvents. For practical applications in food analysis or bioanalysis, water-soluble ECL emitters are highly desired but scarce.[14] In addition, the current ECL investigations on Ru(II) and Ir(III) complexes exclusively focus on tris-bidentate complexes, like $[Ru(bpy)_3]^{2+}$ and $[Ir(ppy)_2(bpy)]^+$ analogues. No ECL studies on bis-terdentate Ir(III) and Ru(II) complexes have been reported, and no reports on the ECL of dinuclear Ir(III) and Ru(II) complexes, either.

In comparison to the tris-bidentate Ir(III)/Ru(II) complexes, the bis-terdentate complexes have higher geometric symmetry, preventing the formation of stereoisomers. Recently, we synthesized and studied various bis-terdentate Ir(III) and Ru(II) complexes.[15-19] Among these complexes, those with higher number of positive charges or containing oligoethoxy substituents showed distinctly improved solubility in aqueous solutions. Especially the dinuclear bisterpyridine complexes holding +6 charges exhibited much better water solubility compared to their mononuclear counterparts. We also revealed that replacing one of the tpy ligands in Ir(III) complexes by cyclometalating ligands altered the emission energies and quantum yields drastically.[15,16,18] However, ECL of the bis-terdentate Ir(III)/Ru(II) complexes has never been exploited.

Herein, we designed and synthesized a series of water-soluble dinuclear Ir(III) and Ru(II) complexes (**1–4** in Scheme 1) for exploration of their ECL performances. These Ir(III) and Ru(II) complexes were end-capped with either tpy or 1,3-di(pyrid-2-yl)-4,6-dimethylbenzene (N^C^N) ligands for adjusting the number of charges on the complexes and for understanding the impact of terminal terdentate ligand on the photophysics and ECL characteristics. Oligoethoxy substituents were introduced

[a] *Department of Chemistry and Biochemistry, North Dakota State University, Fargo, ND 58108-6050, USA*
[b] *School of Integrated Circuit Science and Engineering, Tianjin University of Technology, Tianjin 300384, P. R. China*
Electronic Supplementary Information (ESI) available: NTOs of the singlet and triplet excited states in water and the time-resolved transient absorption spectra of **1-4** in CH_3CN. See DOI: 10.1039/x0xx00000x

to the C9 position of the bridging fluorene motif to further improve the water solubility of these complexes. The photophysical properties of **1**–**4** in aqueous solutions and the ECL behaviors of **1**–**3** (which have good water solubility) in phosphate-buffered saline (PBS) solutions were investigated.

Experimental section

Materials and synthesis

All chemicals and solvents were purchased from VWR International and used directly without further purification unless otherwise noted. Silica gels (60 Å, 230–400 mesh) and activated neutral aluminium oxide (Brockmann I) gels used for column chromatography were obtained from Sorbent Technology. The synthetic routes for complexes **1**–**4** are illustrated in Scheme 1. The precursor compounds 2,7-bis(4,4,5,5-tetramethyl-1,3,2-dioxaborolan-2-yl)-9,9-di(1-(2-(2-methoxyethoxy)ethoxy)ethyl)fluorene,[20,21] (4'-phenyl-2,2':6',2''-terpyridine)$IrCl_3$,[22] {[2,2'-(4,6-dimethyl-1,3-phenylene)bispyridine]$IrCl_2$}$_2$,[23] (4'-phenyl-2,2':6',2''-terpyridine)$RuCl_3$,[24] and [2,2'-(4,6-dimethyl-1,3-phenylene)bispyridine]Ru$(CH_3CN)_3$[25] were prepared according to the established procedures. The synthesized complexes **1**–**4** were characterized by ^{1}H NMR spectroscopy, electrospray ionization high-resolution mass spectrometry (ESI-HRMS), and elemental analysis. The ^{1}H NMR spectra were acquired on a 400 or 500-MHz Varian Oxford VNMR spectrometer, and the spectra are provided in ESI Figs. S1-S4. ESI-HRMS analyses were conducted on a Bruker BioTOF III mass spectrometer. Elemental analyses were carried out by NuMega Resonance Laboratories, Inc. (San Diego, CA).

L1. In a 100 mL round-bottom flask, 2,7-bis(4,4,5,5-tetramethyl-1,3,2-dioxaborolan-2-yl)-9,9-di(1-(2-(2-methoxyethoxy)ethoxy)ethyl)fluorene (710 mg, 1 mmol), 4'-bromo-2,2':6',2''-terpyridine (653 mg, 2.1 mmol), and $Pd(PPh_3)_4$ (116 mg, 0.1 mmol) were mixed in degassed toluene (30 mL) and 2 M K_2CO_3 aqueous solution (10 mL). The obtained mixture was heated to reflux under nitrogen atmosphere for 12 h. After cooling to room temperature, the volatiles were evaporated in vacuo to give a brown residue. The crude product was purified by column chromatography (neutral alumina gel, CH_2Cl_2/ethyl acetate gradient (100:0 to 50:50 (v/v)) to afford the pure product as a pale-yellow solid (760 mg, 83%). ^{1}H NMR (500 MHz, $CDCl_3$) δ 8.82 (d, J = 1.5 Hz, 4H), 8.78 (d, J = 4.7 Hz, 4H), 8.71 (s, 2H), 8.69 (s, 2H), 7.97 (d, J = 5.8 Hz, 4H), 7.94–7.87 (m, 6H), 7.42–7.35 (m, 4H), 3.47–3.35 (m, 4H), 3.42–3.33 (m, 8H), 3.29–3.16 (m, 10H), 2.86 (t, J = 7.6 Hz, 4H), 2.60 (t, J = 7.0 Hz, 4H).

General procedure for the synthesis of complexes 1–4. A suspension of **L1** (46 mg, 0.05 mmol) and the corresponding precursor, (4'-phenyl-2,2':6',2''-terpyridine)$IrCl_3$ (**1**, 0.1 mmol), {[2,2'-(4,6-dimethyl-1,3-phenylene)bispyridine]$IrCl_2$}$_2$ (**2**, 0.05 mmol), (4'-phenyl-2,2':6',2''-terpyridine)$RuCl_3$ (**3**, 0.1 mmol), or [2,2'-(4,6-dimethyl-1,3-phenylene)bispyridine]Ru$(CH_3CN)_3$ (**4**, 0.1 mmol) in 10 mL degassed ethylene glycol (EtOH for **4**) was stirred at reflux in dark under a nitrogen atmosphere for 24 h (3 h for **4**). After cooling to room temperature, saturated aqueous NH_4PF_6 (10 mL) was added to make the crude product precipitate out. The solid was collected and purified by column chromatography on alumina gel eluted with CH_2Cl_2 to remove the unreacted ligand, followed by an acetone/water gradient (100:0 to 95:5 (v/v)). Finally, a metathesis reaction from hexafluorophosphate to chloride ion was executed to obtain the title complexes by passing an anionic ion-exchange resin.

1. Red solid (65 mg, 61%). ^{1}H NMR (400 MHz, D_2O) δ 9.40 (d, J = 9.3 Hz, 4H), 9.28 (s, 2H), 9.26 (s, 2H), 8.92 (t, J = 9.2 Hz, 4H), 8.86–8.78 (m, 4H), 8.54 (s, 2H), 8.45–8.17 (m, 16H), 7.95–7.73 (m, 14H), 7.67–7.54 (m, 8H), 3.67 (s, 6H), 3.51 (d, J = 4.1 Hz, 4H), 3.39–3.33 (m, 4H), 3.32–3.28 (m, 4H), 3.26 (d, J = 4.0 Hz, 4H), 3.24–3.18 (m, 4H), 2.96–2.82 (m, 4H). ESI-HRMS (m/z, in methanol): calcd. for $[C_{99}H_{86}Ir_2N_{12}O_6]^{6+}$, 320.7678; found, 320.7674. Anal. Calcd. (%) for $C_{99}H_{86}Cl_6Ir_2N_{12}O_6{\cdot}12H_2O{\cdot}2CH_2Cl_2$: C, 48.08; H, 4.55; N, 6.66. Found: C, 48.23; H, 4.55; N, 6.36.

2. Brownish solid (68 mg, 69%). ^{1}H NMR (400 MHz, D_2O) δ 9.28 (s, 4H), 8.74 (d, J = 8.0 Hz, 4H), 8.47 (s, 2H), 8.44–8.23 (m, 8H), 8.12 (t, J = 7.7 Hz, 4H), 7.89 (t, J = 7.7 Hz, 4H), 7.60 (d, J = 5.4 Hz, 4H), 7.55 (d, J = 5.5 Hz, 4H), 7.44 (s, 2H), 7.36–7.26 (m, 4H), 7.09–6.93 (m, 4H), 3.67 (s, 6H), 3.46 (s, 4H), 3.32 (d, J = 4.7 Hz, 4H), 3.28 (d, J = 4.3 Hz, 4H), 3.23–3.20 (m, 4H), 3.18 (s, 4H), 3.00 (s, 12H), 2.89–2.85 (m, 4H). ESI-HRMS (m/z, in methanol): calcd. for $[C_{93}H_{86}Ir_2N_{10}O_6]^{4+}$, 456.1502; found, 456.1508. Anal. Calcd. (%) for $C_{93}H_{86}Cl_4Ir_2N_{10}O_6{\cdot}11H_2O{\cdot}2CH_2Cl_2$: C, 48.70; H, 4.57; N, 5.80. Found: C, 48.89; H, 4.84; N, 6.00.

3. Red solid (69 mg, 70%). ^{1}H NMR (500 MHz, D_2O) δ 9.21 (s, 4H), 9.10 (s, 4H), 8.74 (d, J = 8.2 Hz, 4H), 8.67 (d, J = 7.8 Hz, 4H), 8.48 (s, 2H), 8.39–8.34 (m, 4H), 8.22 (d, J = 7.8 Hz, 4H), 8.06–7.91 (m, 8H), 7.85–7.78 (m, 4H), 7.75 (td, J = 7.3, 1.3 Hz, 2H), 7.60–7.46 (m, 8H), 7.23 (t, J = 6.0 Hz, 8H), 3.68 (s, 6H), 3.45–3.43 (m, 4H), 3.37 (d, J = 1.9 Hz, 4H), 3.32–3.31 (m, 4H), 3.24–3.22 (m, 4H), 3.13 (d, J = 1.7 Hz, 4H), 2.89–2.86 (m, 4H). ESI-HRMS (m/z, in methanol): calcd. for $[C_{99}H_{86}N_{12}O_6Ru_2]^{4+}$, 435.6231; found, 435.6225. Anal. Calcd. (%) for $C_{99}H_{86}Cl_4N_{12}O_6Ru_2{\cdot}10H_2O{\cdot}CH_2Cl_2$: C, 55.71; H, 4.74; N, 7.44. Found: C, 55.89; H, 5.07; N, 7.82.

4. Purple solid (74 mg, 87%). ^{1}H NMR (400 MHz, DMSO-d_6) δ 9.61 (s, 4H), 9.10 (d, J = 7.9 Hz, 4H), 8.87 (s, 2H), 8.68 (d, J = 8.0 Hz, 2H), 8.37 (d, J = 8.0 Hz, 2H), 8.26 (d, J = 8.4 Hz, 4H), 7.89 (t, J = 7.8 Hz, 4H), 7.67 (t, J = 7.9 Hz, 4H), 7.17 (dd, J = 12.0, 5.6 Hz, 8H), 7.08 (d, J = 8.3 Hz, 6H), 6.81 – 6.68 (m, 4H), 3.30 (s, 4H), 3.30 – 3.27 (m, 4H), 3.27 – 3.22 (m, 4H), 3.08 (s, 6H), 2.98 (s, 12H), 2.95 – 2.81 (m, 8H), 2.81 – 2.63 (m, 4H). ESI-HRMS (m/z, in methanol): calcd. for $[C_{93}H_{86}N_{10}O_6Ru_2]^{2+}$, 821.24; found, 821.24. Anal. Calcd. (%) for $C_{93}H_{86}Cl_2N_{10}O_6Ru_2{\cdot}7H_2O$: C, 60.74; H, 5.48; N, 7.62. Found: C, 60.57; H, 5.48; N, 7.69.

Photophysical studies

The UV-vis absorption spectra of **1**–**4** were measured at room temperature on a Varian Cary 50 spectrophotometer. The steady-state emission spectra were collected on a HORIBA FluoroMax-4 fluorometer/phosphorometer. The emission quantum yields of **1**–**4** were measured in degassed aqueous solutions (the aqueous solution of **4** contained 5% DMSO (v/v)) using the relative actinometry,[26] with a deaerated acetonitrile solution of $[Ru(bpy)_3]Cl_2$ being employed as the reference (Φ_{em} = 0.097, λ_{ex} = 436 nm).[27] The time-resolved nanosecond

transient difference absorption (TA) spectra and triplet lifetimes of **1**–**4** were measured in nitrogen-purged aqueous solutions and acetonitrile solutions on an Edinburgh LP920 laser flash photolysis spectrometer. The sample solutions were excited by 355 nm light from a Nd:YAG laser (Quantel Brilliant, 4.1 ns, 1 Hz).

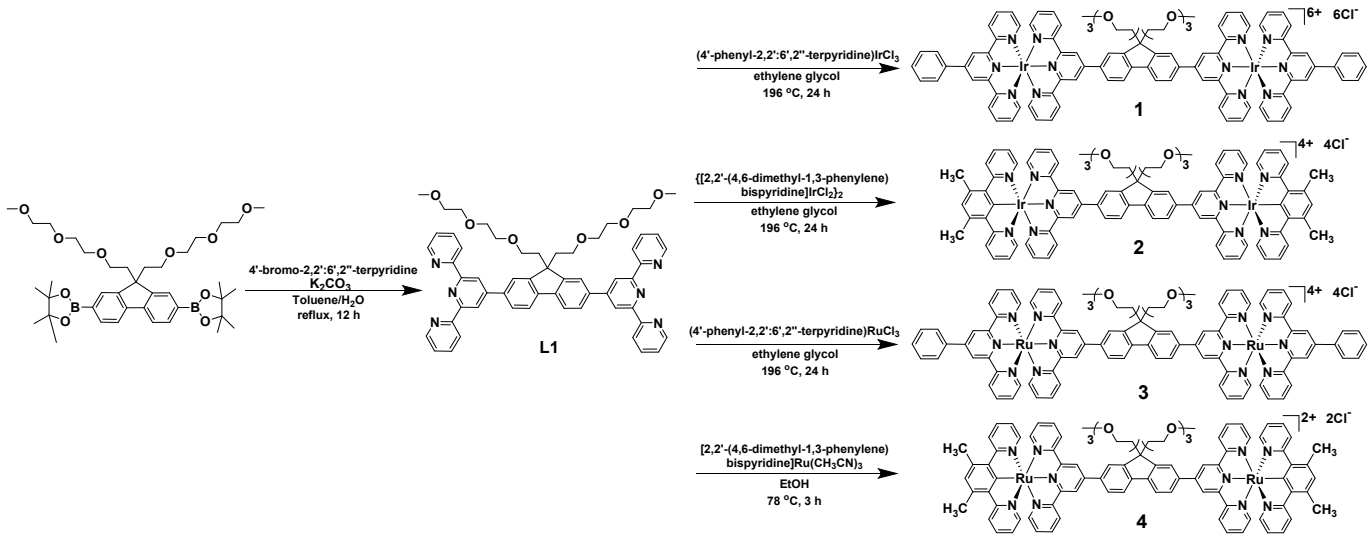

Scheme 1 Structures and synthetic routes for complexes **1**–**4**.

Computational methodology

All calculations were performed using Gaussian-16 software package.[28] The ground-state geometries of all complexes were optimized based on the density functional theory (DFT) level[29] applying the Perdew-Burke-Ernzerhof (PBE0)[30] hybrid exchange-correlation functional and the mixed basis set, with the LANL2DZ basis set[31] being used for Ir(III) and Ru(II) metal centers and all other atoms of the complexes being treated using the 6-31G* basis set.[32] Solvation effects were included using the conductor-like polarizable continuum model (CPCM)[33] model choosing water as a solvent in order to correspond to experimental data.

Absorption spectra were reproduced based on 150 optical transitions obtained from the linear response time-dependent DFT (TD-DFT)[34] calculations using the same methodology as for the ground state calculations. The spectral profile was simulated using Gaussian function with the line width of 0.08 eV providing the thermal broadening comparable to experimental spectra. In addition, Becke 3-parameter Lee-Yang-Parr (B3LYP)[35] functional was tested along with the PBE0 functional. Both functionals provided qualitatively similar spectral profiles agreeing with experimental spectra, except for a consistent blue shift that was the more pronounced for the Ru(II) complexes **3** and **4**. Comparison with the experimental absorption spectra indicated that the PBE0 functional well reproduced the experimental absorption spectra of complexes **1** and **2** with the Ir(III) metal center, while the B3LYP functional was more accurate for reproducing absorption spectra of complexes **3** and **4** with the Ru(II) metal center. This difference in the choices of the density functionals were justified[36,37] in literature reports for Ir(III)[38-41] and Ru(II)[17,39,42,43] complexes.

For calculations of the phosphorescence energies, several lower-energy states with the triplet spin multiplicity were optimized along their excited surface potential using analytical gradient TDDFT method[44] applying the same methodology as in the ground state calculations. The final phosphorescence energies were chosen to provide the best agreement with experimental emission spectra. The localization/delocalization and charge transfer properties of electron-hole pairs contributing to the singlet and triplet optical transitions were illustrated using the natural transition orbitals (NTOs) generated from the unitary transformation of the transition density matrices.[45] NTOs were visualized in VMD[46] visualization code with a 0.02 iso value.

ECL

The electrochemical experiments were carried out using a three-electrode system, where carbon paper, Ag/AgCl electrode, and platinum wire were applied as the working, reference, and counter electrode, respectively. With tripropylamine (TPrA, 200 μL) as the co-reactant, the cell contained PBS buffer (200 μL, 10 mM, pH = 7) and sample solution (200 μL, 5 mM) was used for cyclic voltammetry (CV) study on MPI-EII (Remex Electronic Instrument Co., Ltd.). The CV measurements were conducted in a voltage range of -0.5 V to 0.5 V with a 900 V photomultiplier and 80 mv·s^{-1} scan speed.

Results and discussion

Electronic absorption

The UV–vis absorption spectra of **1**–**4** were investigated in aqueous solutions (with 10% DMSO being added in the aqueous solution of **4** to improve its solubility). The absorption band maxima and extinction coefficients are tabulated in Table 1. As illustrated in Fig. 1, intense absorption bands with extinction coefficients of >78000 M^{-1}·cm^{-1} appear at <350 nm for all complexes, which can be attributed to the spin-allowed ligand-localized $^1\pi,\pi^*$ transitions. Based on the NTOs (Table S1) for the major transitions contributing to these absorption bands, the

origin of these bands is ascribed to the $^1\pi,\pi^*$ transitions localized on the bridging ligand. All complexes feature another major absorption band(s) at 350-450 nm, which are less intense, broader, and structureless compared to the high-energy absorption bands at <350 nm. NTOs in Table S1 indicate that these bands emanate predominately from the bridging ligand-localized $^1\pi,\pi^*$/^{1}ILCT (intraligand charge transfer) transitions, mixed with $^1\pi,\pi^*$/^{1}LLCT (ligand-to-ligand charge transfer) /^{1}MLCT (metal-to-ligand charge transfer) transitions associated with the terpyridine ligands. Beyond 450 nm, the two Ir(III) complexes **1** and **2** possess weakly absorbing tails with a very weak absorption band ($\varepsilon \leq 1150$ M^{-1}·cm^{-1}) emerging at ca. 573 nm (see inset in Fig. 1). According to the NTOs in Table 2, the absorption in this region mainly stems from the ^{1,3}MLCT (metal-to-ligand charge-transfer) / ^{1,3}LLCT transitions. In contrast, the two Ru(II) complexes **3** and **4** display very strong absorption band(s) at 497 nm and 521/572 nm, respectively. Complex **3** also exhibits a shoulder at ca. 567 nm. With reference to the NTOs contributing to the major transitions in this region, these bands are predominantly ascribed to the bridging ligand localized $^1\pi,\pi^*$ transitions admixing with ^{1}MLCT/^{1}LLCT transitions. These much red-shifted low-energy $^1\pi,\pi^*$/^{1}CT (charge transfer) absorption bands in the Ru(II) complexes **3** and **4** can be ascribed to the weaker ligand field strength of the Ru(II) ion in comparison to that of the Ir(III) ion, leading to a smaller crystal field splitting energy of the *d* orbitals in Ru(II)-based analogues.[39] Consequently, the *d* orbitals in the Ru(II) complexes are high-lying, making a significant contribution to the holes of the electronic transitions corresponding to the absorption band(s) at > 450 nm in **3** and **4**. In comparison to the well-studied mononuclear Ru(tpy)$_2^{2+}$ complex,[47] the $^1\pi,\pi^*$/^{1}CT band in the dinuclear complex **3** exhibits a 21-nm red shift and the molar extinction coefficient is 3.7 folder larger, which reflects the more delocalized LUMO crossing the π-expansive bridging ligand. Both the energy and molar extinction coefficient of this $^1\pi,\pi^*$/^{1}CT band in **3** resemble those of the dinuclear (tpy)Ru(tpy-Ph-tpy)Ru(tpy)$^{4+}$ complex.[48]

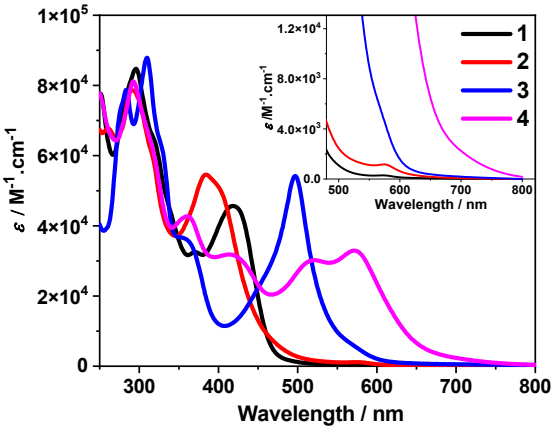

Fig. 1 UV–vis absorption spectra of **1**–**4** at room temperature in aqueous solutions (with 10% (v/v) DMSO being added in the solution of **4**).

Comparing the absorption bands of **1** and **2** reveals that replacing the distal tpy ligands in **1** by the N^C^N ligands in **2** caused a blue shift of the absorption band at 350-450 nm in **2** but increased the molar extinction coefficient of the absorption bands at > 450 nm with respect to the corresponding bands in **1** owing to the stronger σ-donating ability of the N^C^N ligand. In contrast, substituting the terminal tpy ligands in the Ru(II) complex **3** with the N^C^N ligands red-shifted and distinctly resolved this absorption band into two bands at 521 and 572 nm in **4**.

Photoluminescence

The photoluminescence of **1**–**4** was studied in deoxygenated aqueous solutions. Fig. 2 displays the normalized emission spectra of **1**–**3** and the emission band maxima and lifetimes are compiled in Table 1. The emission of **4** was too weak to be monitored. The emission spectra of **1**–**3** are much red-shifted compared to their corresponding excitation wavelengths, and the emission intensity is prone to oxygen quenching accompanied by a relatively long lifetime for **1** and **2**. These characteristics suggest phosphorescence for the observed emission, which is a common feature for Ir(III) and Ru(II) complexes.

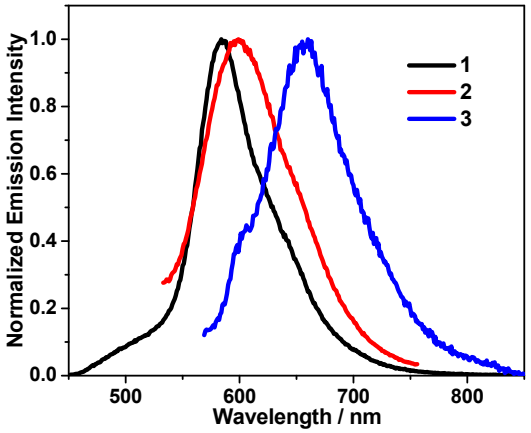

Fig. 2 Emission spectra of **1** (λ_{ex} = 419 nm), **2** (λ_{ex} = 385 nm), and **3** (λ_{ex} = 497 nm) at room temperature in deoxygenated aqueous solutions ($c = 1 \times 10^{-5}$ mol·L^{-1}).

The emission spectrum of **1** exhibited somewhat vibronic structure along with a much longer emission lifetime and higher quantum yield in comparison to those of **2** and **3**. With reference to the reported dinuclear Ir(III) complex with the similar bridging ligand and the NTOs for the T_2 state of this complex in Table 3, the emitting state of this complex is ascribed predominantly to the bridging ligand-centered $^3\pi,\pi^*$ state mixed with minor ^{3}CT character.[15] Based on the NTOs, the emitting states for complexes **2** and **3** are also dominated by the bridging ligand-localized $^3\pi,\pi^*$ states but with more ^{3}MLCT characters. The involvement of more charge transfer characters in the emitting states of **2** and **3** led to much reduced emission lifetimes and lower emission quantum yields. Replacing the terminal tpy ligands by the N^C^N ligands slightly red-shifted the emission band maximum of **2** to 602 nm compared to that of **1** (585 nm), which agrees with the trend observed in their ^{1}CT absorption bands. For the dinuclear Ru(II) complex **3**, more

involvement of the ^{3}MLCT character in the emitting state led to a more red-shifted emission band accompanied by a much lower emission quantum yield with respect to its corresponding Ir(III) complex **1**. The emission lifetime of **3** was too short to be monitored on our instrument. While for complex **4** bearing the N^C^N terminal ligands, its emission was too weak to be detected in aqueous solutions.

Table 1 Electronic absorption and emission for complexes **1**–**4**.

	λ_{abs}/nm (log ε)[a]	λ_{em}/nm (τ_{em}/ns); Φ_{em}[b]	λ_{T1-Tn}/nm (τ_{TA}/ns)	
1	296 (4.93), 370 (4.51), 419 (4.66), 573 (2.47)	585 (2710); 0.034	768 (38830)[c]	768 (2920)[d]
2	291 (4.89), 385 (4.74), 573 (3.06)	602 (300); 0.0065	795 (300)[c]	705 (20)[d]
3	283 (4.90), 310 (4.94), 356 (4.56), 497 (4.73)	657 (-)[e]; ＜0.0001	676 (-)[c,f]	676 (-)[d,f]
4	292 (4.91), 360 (4.63), 412 (4.50), 521 (4.48), 572 (4.52)	-[e]	767 (-)[c,f]	767 (-)[d,f]

[a]Absorption band maxima (λ_{abs}) and molar extinction coefficients (ε) recorded in aqueous solution (with 10% DMSO for **4**) at room temperature. [b]Emission band maxima (λ_{em}), lifetimes (τ_{em}), and quantum yields (Φ_{em}) measured in aqueous solution (c = 1 × 10^{-5} mol·L^{-1}) at room temperature with $Ru(bpy)_3Cl_2$ (in degassed acetonitrile, Φ_{em} = 0.097, λ_{ex} = 436 nm) as the reference. [c]Nanosecond TA band maxima (λ_{T1-Tn}) and triplet excited-state lifetimes (τ_{TA}) measured in aqueous solution (with 10% DMSO for **4**) at room temperature. [d]Recorded in acetonitrile. [e]Too weak to be measured. [f]The lifetime was too short to be accurately measured on our instrument.

Table 2 Natural transition orbitals (NTOs) of the transitions contributing to the low-energy absorption bands of **1**-**4** in H_2O. Calculations were carried out using TDDFT theory and LAN2dz/6-31G* basis set. PBE0 functional was used for calculations of **1** and **2**, and B3LYP for **3** and **4**.

	S_n and properties	Hole	Electron
1	S_1 440 nm *f*=1.4350 S_2 406 nm *f*=0.0112	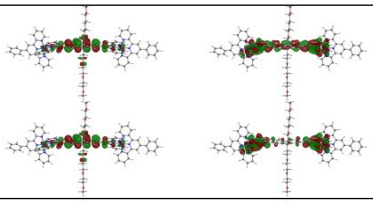	
2	S_1 439 nm *f*= 0.0002 S_2 439 nm *f*= 0.0003 S_3 412 nm *f*= 1.4083	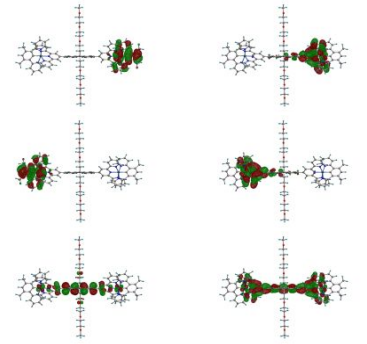	
3	S_1 476 nm *f*= 0.0010 S_9 460 nm *f*= 1.5084 S_{19} 413 nm *f*= 0.4803	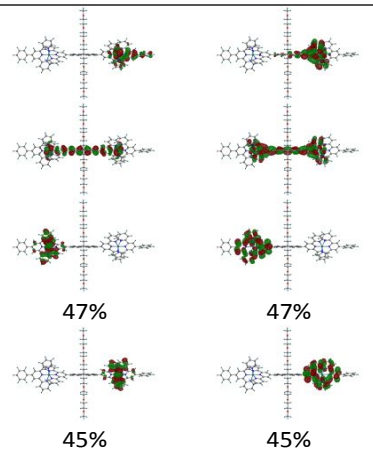	
		47%	47%
		45%	45%
4	S_1 622 nm *f*= 0.0000 S_7 521 nm *f*= 0.3621 S_{13} 464 nm *f*= 0.7618	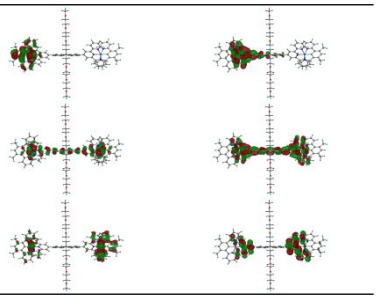	

Table 3 Natural transition orbitals (NTOs) of the Tn states of **1**-**3** in H_2O. Calculations were carried out using analytical TDDFT method and LAN2dz/6-31G* basis set. PBE0 functional was used for the calculations.

	T_n/nm	HOTO	LUTO
1	T_1 614 T_2 545	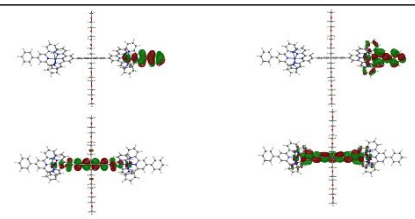	
2	T_1 586	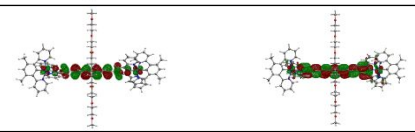	
3	T_1 652	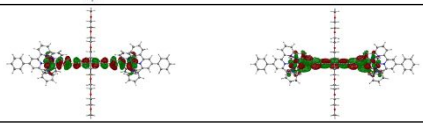	

Transient absorption (TA)

To further understand the triplet excited-state properties of **1**–**4**, nanosecond TA were investigated in degassed aqueous solutions (with 10% DMSO for **4**) and in acetonitrile. The obtained time-resolved TA spectra are presented in Fig. 3 and Fig. S8, respectively. The TA band maxima and triplet lifetimes are tabulated in Table 1. As displayed in Fig. 3, the TA spectra of **1**, **3**, and **4** consist of bleaching bands that are in accordance with their respective visible absorption bands and broad

positive absorption bands ranging from 456 to 800 nm for **1**, 423-800 nm for **2**, and 550-800 nm for **3**. The spectral features of **1** and **2** are similar to those of our previously reported Ir(III) complexes bearing the similar bridging and distal ligands, indicating that the transient absorbing excited species can be predominantly assigned to the bridging ligand localized $^3\pi,\pi^*$ states for **1**, and mixed $^3\pi,\pi^*/^3$CT state for **2**. For the Ru(II) complexes **3** and **4**, their TA spectral features resembled each other and the TA signals decayed rapidly, which are similar to that observed for their emission decays. Therefore, the excited states giving rise to the monitored signals are likely the $^3\pi,\pi^*/^3$MLCT T_1 states for these two complexes. It is interesting to note that the lifetime of **1** monitored from the decay of the TA signals, i.e., 38.83 μs, is one order of magnitude longer than that obtained from the decay of emission signals (2.71 μs) in aqueous solutions. Although rare, this phenomenon is not unprecedent in transition-metal complexes. Some Ir(III), Ru(II), and Pt(II) complexes have been reported to possess a high-lying emissive excited state and a non-emissive, long-lived T_1 state.[40,49,50]

Another general trend revealed is that the two Ir(III) complexes demonstrated much longer-lived T_1 states than their corresponding Ru(II) complexes. This characteristic can be ascribed to the stronger ligand-field strength of the Ir(III) ion with respect to that of the Ru(II) ion, which leads to a much larger crystal field splitting and results in deep-situated metal-based *d* orbitals in the Ir(III) complexes.[39] Consequently, contributions of the *d* orbitals to the frontier molecular orbitals are significantly reduced in the Ir(III) complexes, and the triplet lifetimes of the Ir(III) complexes are much longer than those of their corresponding Ru(II) complexes. This phenomenon was reported by our group for the mononuclear Ir(III) and Ru(II) complexes,[39] which has been found to be true in the dinuclear complexes in this work. Additionally, replacing the terminal terpyridine ligands by the N^C^N ligands decreased the triplet lifetimes and led to much weaker TA signals in **2** and **4**.

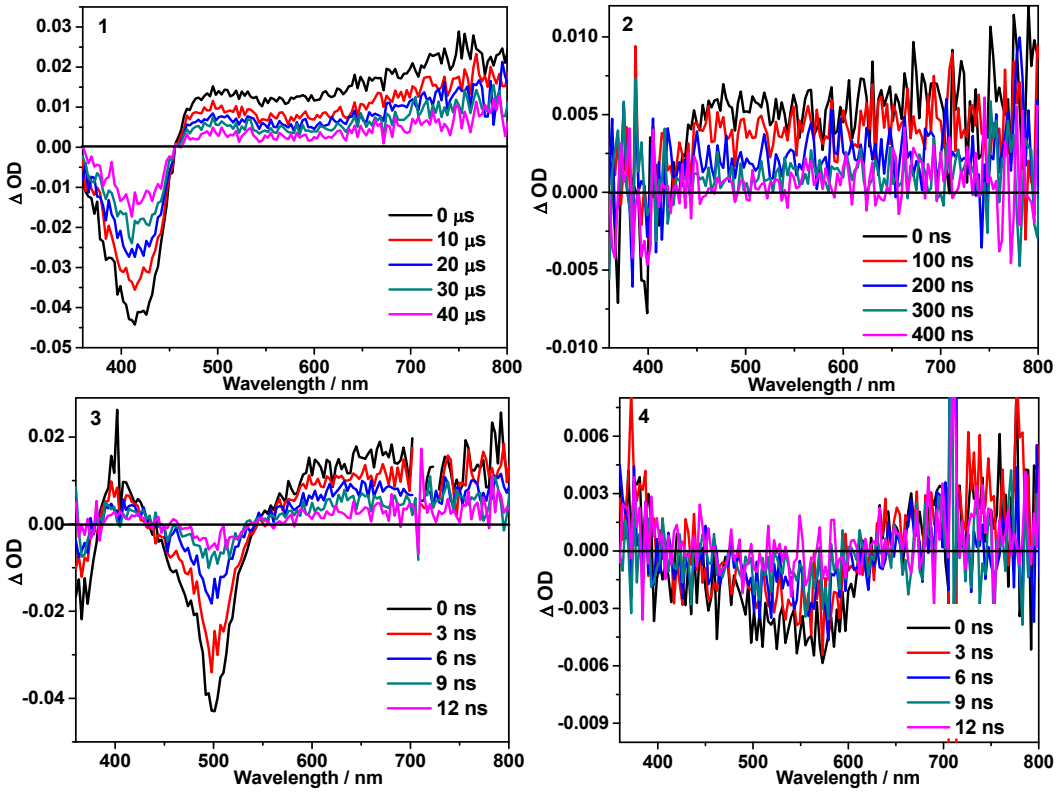

Fig. 3 Time-resolved ns TA spectra of **1**–**4** in aqueous solutions (with 10% DMSO for **4**) at room temperature after 355 nm laser pulse excitation. $A_{355\ nm}$ = 0.4 in a 1-cm cuvette.

ECL performances

To investigate the electrochemical behaviours of **1**–**3**, cyclic voltammogram (CV) studies were performed in PBS buffer solutions, and the recorded profiles are shown in Fig. 4a. The area of the CVs is expressed as the capacitance of the material, while the capacitance is expressed as the ability of the material to store electrons. Therefore, the smaller the area, the weaker the material's ability to store electrons. In other words, the substance has a relatively strong ability to lose electrons. From the perspective of ECL, it is easier to change from the ground state to the excited state to produce a stronger ECL signal. Fig. 4a shows that the CV area of **3** is the smallest. Therefore, **3** may show stronger ECL signal intensities under the same conditions.

The ECL studies were carried out in PBS solutions containing tripropylamine (TPrA) as the co-reactant. The corresponding potentials giving rise to emission signals, i.e., -0.2 and -0.4 V for **1**, and -0.1 V for **2** and **3**, were found from the ECL intensity vs. voltage curves (Fig. 4c). Subsequently, the applied potentials

were set at the appropriate values giving rise to the maximum emission signals, and the recorded ECL profiles were collected as a function of time (Fig. 4b). Interestingly, much higher ECL signals were generated by **3** with good stability and reproducibility, and the obtained Φ_{ECL} follows the trend of **3**＞**1**＞**2** (Fig. 4d). In addition, the error rate of ECL signal intensity of the three complexes is low in 10 cycles, which is 5.2%, 8.5%, and 10.8% for sample **1, 2** and **3**, respectively. While the relative ECL intensity of **1** and **2** is consistent with their photoluminescence quantum yield, the very low photoluminescence quantum yield and short-lived emitting state of **3** in an aqueous solution as discussed in the photoluminescence section make it unexpected that **3** gave rise to the strongest ECL. To understand the unusually high ECL signals of **3**, the origins of the ECL in these complexes are analyzed.

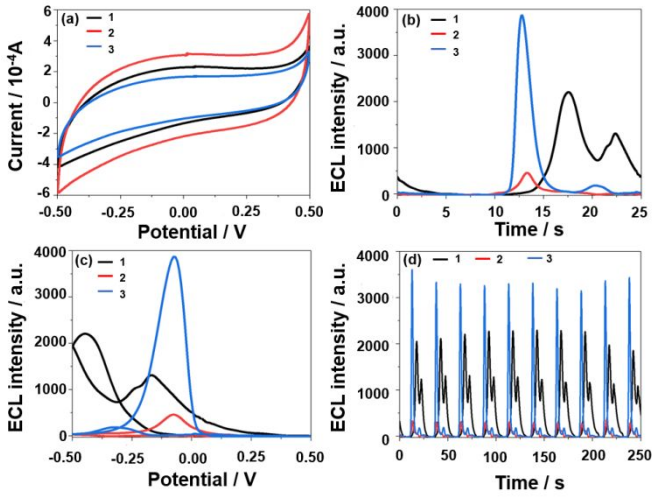

Fig. 4 (a) CV curves, (b) ECL intensity over time, (c) ECL intensity as a function of voltage, and (d) the luminescence stability of **1** (black), **2** (red) and **3** (blue).

According to the ECL mechanism described for other Ir(III) and Ru(II) complexes reported in the literature,[1-4] it is believed that the ECL for **1**-**3** was produced via the sequential reactions depicted in Scheme 2. The complexes (R) and TPrA are reversibly oxidized on the surface of the electrode to generate R^+ cations and TPrA$^\bullet$ radicals. R^+ can interact irreversibly with TPrA$^\bullet$ by diffusing to afford an excited species, R*, which instantaneously returns to the ground state and release the excited energy as photons to generate ECL. As shown in Fig. 4a, complex **3** exhibited a narrower CV curve, suggesting that it can readily release electrons to generate the R^+ and TPrA$^\bullet$ species. The curve area of these complexes decreases in the order of **3**＞**1**＞**2**, which is in line with the trend of their ECL intensities.

$R - e^- \rightarrow R^+$ (1)
$TPrA - e^- \rightarrow [TPrA]^{+\cdot} \rightarrow TPrA^\bullet + H^+$ (2)
$R^+ + TPrA^\bullet \rightarrow R^* +$ other products (3)
$R^* \rightarrow R + h\nu$ (4)

Scheme 2. ECL generation mechanism for **1**–**3**. R represents the emitter complex.

Conclusions

Four water-soluble dinuclear Ir(III) and Ru(II) complexes with two $M(tpy)_2$ or M(tpy)(N^C^N) units (M = Ir or Ru) tethered by a fluorenyl motif were synthesized and their photophysical properties systematically investigated. The influence of the different terminal-capping ligands and metal centers on their photophysical properties was assessed by employing various spectroscopic techniques and TD-DFT calculations. In comparison to their corresponding terminally tpy-capped complexes **1** and **3**, complexes **2** and **4** with the N^C^N terminal ligands showed considerably red-shifted absorption bands in their UV-vis absorption spectra, owing to the stronger σ-donating ability of the N^C^N ligand compared to that of tpy. On the other hand, the two Ru(II) complexes **3** and **4** exhibited bathochromically shifted low-energy absorption bands and emission bands due to the increased involvement of the charge transfer characters in their S_1 and T_1 states. The reduced energies of the emitting states induced by either the N^C^N ligand or the Ru metal ion decreased the emission quantum yields and shortened the triplet excited state lifetimes following the energy gap law. All complexes exhibited positive triplet excited-state absorption bands in the red to the NIR regions, with the two complexes bearing the tpy terminal-capped ligands (i. e. **1** and **3**) showing much stronger transient signals than the two complexes with the N^C^N terminal ligands. The transient signals from the two Ir(III) complexes are also stronger than those of their corresponding Ru(II) complexes. Complexes **1**–**3** also manifested ECL in PBS buffer solutions using carbon paper as the working electrode. The intensity of the ECL signals followed the trend of **3**>**1**>**2**. The strong signal of **3** could be ascribed to its ease of oxidation for initiating the electrochemical processes. Generally, the complexes with the tpy terminal ligands showed stronger ECL signals than the one with the N^C^N ligands. These complexes are the first examples of dinuclear Ir(III) and Ru(II) complexes with ECL properties, especially the complexes with $[M(tpy)_2]^{n+}$ motifs demonstrated the potential as water-soluble ECL emitters.

Conflicts of interest

The authors declare no competing financial interest.

Acknowledgements

W. Sun and S. Kilina acknowledge financial support from the National Science Foundation (CHE-1800476) for the synthesis, photophysical, and computational studies of the complexes. We are also grateful to the Center for Computationally Assisted Science and Technology (CCAST) at North Dakota State University for computational resources, which were made possible in part by NSF MRI Award No. 2019077.

Notes and references

1 C. Ma, Y. Cao, X. Gou and J. Zhu, *Anal. Chem.* 2020, **92**, 1, 431–454.

2 W. Miao, *Chem. Rev.*, 2008, **108**, 2506–2553.
3 Z. Liu, W. Qi and G. Xu, *Chem. Soc. Rev.*, 2015, **44**, 3117–3142.
4 L. Hu and G. Xu, *Chem. Soc. Rev.*, 2010, **39**, 3275–3304.
5 J. Y. Kim, S. Cheon, H. Lee, J.-Y. Oh, J.-I. Lee, H. Ryu, Y.-H. Kim and C.-S. Hwang, *J. Mater. Chem. C*, 2017, **5**, 4214–4218.
6 N. Hao and K. Wang, *Anal. Bioanal. Chem.*, 2016, **408**, 7035–7048.
7 E. M. Gross, S. S. Maddipati and S. M. Snyder, *Bioanalysis*, 2016, **8**, 2071–2089.
8 N. E. Tokel and A. J. Bard, *J. Am. Chem. Soc.*, 1972, **94**, 2862–2863.
9 N. E. Tokel-Takvoryan, R. E. Hemingway and A. J. Bard, *J. Am. Chem. Soc.*, 1973, **95**, 6582–6589.
10 X. Zhou, D. Zhu, Y. Liao, W. Liu, H. Liu, Z. Ma and D. Xing, *Nat. Protoc.*, 2014, **9**, 1146–1159.
11 I. K. Jae, I. S. Shin, H. Kim and J. K. Lee, *J. Am. Chem. Soc.*, 2005, **127**, 1614–1615.
12 K. N. Swanick, S. Ladouceur, E. Zysman-Colman and Z. Ding, *Angew. Chem.*, 2012, **124**, 11241–11244.
13 Y. Zhou, K. Xie, R. Leng, L. Kong, C. Liu, Q. Zhang and X. Wang, *Dalton Trans.*, 2017, **46**, 355−363.
14 M. J. Li, P. Jiao, M. Lin, W. He, G. N. Chen and X. Chen, *Analyst*, 2011, **136**, 205–210.
15 B. Liu, S. Monro, L. Lystrom, C. G. Cameron, K. Colón, H. Yin, S. Kilina, S. A. McFarland and W. Sun, *Inorg. Chem.*, 2018, **57**, 9859–9872.
16 B. Liu, S. Monro, Z. Li, M. A. Jabed, D. Ramirez, C. G. Cameron, K. Colón, J. Roque, S. Kilina, J. Tian, S. A. Mcfarland and W. Sun, *ACS Appl. Bio Mater.*, 2019, **2**, 2964–2977.
17 B. Liu, Y. Gao, M. A. Jabed, S. Kilina, G. Liu and W. Sun, *ACS Appl. Bio Mater.*, 2020, **3**, 6025–6038.
18 B. Liu, M. A. Jabed, S. Kilina and W. Sun, *Inorg. Chem.*, 2020, **59**, 8532–8542.
19 C. Lu, W. Xu, H. Shah, B. Liu, W. Xu, L. Sun, S. Y. Qian and W. Sun, *ACS Appl. Bio Mater.*, 2020, **3**, 6865-6875.
20 L. Zhou, X. Bao, Q. Liu, J. Yu, Y. Chen, R. Yang and M. Sun, *J. Appl. Polym. Sci.*, 2014, **131**, 40478.
21 S. Sax, N. Rugen-Penkalla, A. Neuhold, S. Schuh, E. Zojer, E. J. W. List and K. Mu¨llen, *Adv. Mater.*, 2010, **22**,2087–2091.
22 D. N. Chirdon, W. J. Transue, H. N. Kagalwala, A. Kaur, A. B. Maurer, T. Pintauer and S. Bernhard, *Inorg. Chem.*, 2014, **53**, 1487–1499.
23 A. J. Wilkinson, H. Puschmann, J. A. K. Howard, C. E. Foster and J. A. G. Williams, *Inorg. Chem.*, 2006, **45**, 8685–8699.
24 D. Taher, M. E. Thibault, D. DiMondo, M. Jennings and M. Schlaf, *Chem. - A Eur. J.*, 2009, **15**, 10132–10143.
25 Z. Ji and Y. Wu, *J. Phys. Chem. C*, 2013, **117**, 18315–18324.
26 J. N. Demas and G. A. Crosby, *J. Phys. Chem.*, 1971, **75**, 991–1024.
27 K. Suzuki, A. Kobayashi, S. Kaneko, K. Takehira, T. Yoshihara, H. Ishida, Y. Shiina, S. Oishi and S. Tobita, *Phys. Chem. Chem. Phys.*, 2009, **11**, 9850–9860.
28 M. J. Frisch, G. W. Trucks, H. B. Schlegel, G. E. Scuseria, M. A. Robb, J. R. Cheeseman, G. Scalmani, V. Barone, G. A. Peterson and H. Nakatsuji, et al. *Gaussian 16 Rev. C.01*, Wallingford, CT, 2016.
29 A. D. Becke, *J. Chem. Phys.*, 2014, **140**, 18A301-1–18A301-18.
30 J. P. Perdew, K. Burke and M. Ernzerhof, *Phys. Rev. Lett.* 1996, **77**, 3865-3868.
31 P. J. Hay and W. R. Wadt, *J. Chem. Phys.*, 1985, **82**, 270-283.
32 V. A. Rassolov, J. A. Pople, M. A. Ratner and T. L. Windus, *J. Chem. Phys.* 1998, **109**, 1223-1229.
33 M. Cossi, N. Rega, G. Scalmani and V. Barone, *J. Comput. Chem.*, 2003, **24**, 669-681.
34 C. Adamo and D. Jacquemin, *Chem. Soc. Rev.*, 2013, **42**, 845−856.
35 J. Tirado-Rives and W. L. Jorgensen, *J. Chem. Theory Comput.*, 2008, **4**, 297–306.
36 S. Kilina, D. Kilin and S. Tretiak, *Chem. Rev.*, 2015, **115**, 5929–5978.
37 S.-C. Qi, J.-i. Hayashi and L. Zhang, *RSC Adv.*, 2016, **6**, 77375-77395.
38 L. Wang, S. Monro, P. Cui, H. Yin, B. Liu, C. G. Cameron, W. Xu, M. Hetu, A. Fuller, S. Kilina, S. A. McFarland and W. Sun, *ACS Appl. Mater. Interfaces*, 2019, **11**, 3629-3644.
39 L. Wang, P. Cui, B. Liu, S. Kilina and W. Sun, *Dalton Trans.* 2018, **47**, 13776-13780.
40 C. Wang, L. Lystrom, H. Yin, M. Hetu, S. Kilina, S. A. McFarland and W. Sun, *Dalton Trans.*, 2016, **45**, 16366-16378.
41 B. Liu, S. Monro, M. A. Jabed, C. G. Cameron, K. L. Colón, W. Xu, S. Kilina, S. A. McFarland and W. Sun, *Photochem. Photobiol. Sci.*, 2019, **18**, 2381-2396.
42 V. V. Alberta, E. Badaeva, S. Kilina, M. Sykora and S. Tretiak, *J. Lumin.*, 2011, **131**, 1739-1746.
43 E. Badaeva, V. V. Albert, S. Kilina, A. Koposov, M. Sykora and S. Tretiak, *Phys. Chem. Chem. Phys.*, 2010, **12**, 8902-8913.
44 F. Furche and R. Ahlrichs, *J. Chem. Phys.*, 2002, **117**, 7433-7447.
45 R. L. Martin, *J. Chem. Phys.*, 2003, **118**, 4775-4777.
46 W. Humphrey, A. Dalke, K. Schulten, *J. Mol. Graph.*, 1996, **14**, 33-38.
47 E. Jakubikova, W. Chen, D. M. Dattelbaum, F. N. Rein, R. C. Rocha, R. L. Martin and E. R. Batista, *Inorg. Chem.*, 2009, **48**, 10720–10725.
48 J.-P. Collin, P. Lainé, J.-P. Launay and A. Sour, *J. Chem. Soc., Chem. Commun.*, 1993, 434-435.
49 L. Wang, H. Yin, M. A. Jabed, M. Hetu, S. Monro, C. Wang, S. Kilina, S. A. McFarland and W. Sun, *Inorg. Chem.*, 2017, **56**, 3245-3259.
50 R. Liu, N. Dandu, Y. Li, S. Kilina and W. Sun, *Dalton Trans*. 2013, **42**, 4398-4409.

Dalton Transactions

ARTICLE

Table of Contents Entry

The photophysics and electrochemiluminescence properties of four water-soluble dinuclear Ir(III) and Ru(II) complexes terminally-capped by 4′-phenyl-2,2′:6′,2′′-terpyridine (tpy) or 1,3-di(pyrid-2-yl)-4,6-dimethylbenzene (N^C^N) ligands and linked by a 2,7-bis(2,2′:6′,2′′-terpyridyl)fluorene with oligoether chains on C9 are impacted by the tpy or N^C^N ligands and by the metal centers.